Inorganic Chemistry

Article

pubs.acs.org/IC

Excited States and Luminescent Properties of UO_2F_2 and Its Solvated Complexes in Aqueous Solution

Jing Su,*[,†,§] Zheming Wang,*[,‡] Duoqiang Pan,[‡,∥] and Jun Li*[,‡,§]

[†]Division of Nuclear Materials Science and Engineering, Shanghai Institute of Applied Physics, and Key Laboratory of Nuclear Radiation and Nuclear Energy Technology, Chinese Academy of Sciences, Shanghai 201800, China

[‡]William R. Wiley Environmental Molecular Sciences Laboratory, Pacific Northwest National Laboratory, P. O. Box 999, Richland, Washington 99352, United States

[§]Department of Chemistry and Laboratory of Organic Optoelectronics and Molecular Engineering of the Ministry of Education, Tsinghua University, Beijing 100084, China

[∥]Radiochemistry Laboratory, School of Nuclear Science and Technology, Lanzhou University, Lanzhou 730000, Gansu, China

ABSTRACT: The electronic absorption and emission spectra of free UO_2F_2 and its water solvated complexes below 32 000 cm^{-1} are investigated at the levels of ab initio CASPT2 and CCSD(T) with inclusion of scalar relativistic and spin−orbit coupling effects. The influence of the water coordination on the electronic spectra of UO_2F_2 is explored by investigating the excited states of solvated complexes $(H_2O)_nUO_2F_2$ (n = 1−3). In these uranyl complexes, water coordination is found to have appreciable influence on the $^3\Delta$ ($\Omega = 1_g$) character of the luminescent state and on the electronic spectral shape. The simulated luminescence spectral curves based on the calculated spectral parameters of $(H_2O)_nUO_2F_2$ from CCSD(T) approach agree well with experimental spectra in aqueous solution at both near-liquid-helium temperature and room temperature. The possible luminescence spectra of free UO_2F_2 in gas phase are predicted on the basis of CASPT2 and CCSD(T) results, respectively, by considering three symmetric vibration modes. The effect of competition between spin−orbit coupling and ligand field repulsion on the luminescent state properties is discussed.

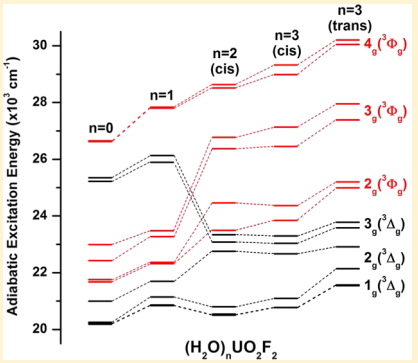

1. INTRODUCTION

Uranyl compounds exhibit characteristic optical properties in absorption and emission. The history of scientific study on this ubiquitous UO_2^{2+} species can be traced back to the middle time of last century.[1] The fluorescence spectra are characterized by many vibrational progressions based on a common electronic origin, where vibrational progression in the O−U−O symmetric stretching mode is dominated.[2] Such a feature has been utilized to study speciation of uranyl in natural and artificial environments by virtue of the time-resolved laser-induced fluorescence (TRLIF) experiment technique.[3−7] TRLIF as a powerful tool is important for molecular-level understanding of the interaction of actinides with various inorganic and organic/biochemical ligands and provides the basic information for handling actinide contaminations in the environment and in biological systems.[8−11] Besides, the intensity distribution of fluorescence spectra changes as the ligand coordinated to uranyl ion varies. Therefore, the exploration of the coordination structure, electronic structure, and excited states of uranyl compounds is essential to understanding of the nature of the fluorescence spectra.

We have recently investigated the vibration-resolved luminescence spectra of uranyl−glycine−water complexes in solution[12] and that of UO_2Cl_2 in an argon matrix,[13] as well as a relevant $UO_2X_3^-$ (X = F, Cl, Br, I)[14] and $NpO_2Cl_4^{2-}$ complex.[15] Spin−orbit (SO)-coupled ab initio wave function theory (WFT) approaches such as coupled clusters with -single, -double, and perturbative-triple substitutions (CCSD(T)), complete-active-space self-consistent field (CASSCF), and multiconfigurational many-electron second-order perturbation theory (CASPT2) have proven their strength in reproducing the experimental spectral shapes and refining the assignments. In this paper, we will investigate UO_2F_2 and its solvated compounds in aqueous solution with a detailed study of the influence of coordinated ligands on the uranyl luminescence spectra. The purpose of the present paper is the theoretical analysis of geometric and electronic structure and the computational simulation of luminescence spectra of UO_2F_2 and its water-solvated compounds $(H_2O)_nUO_2F_2$ (n = 1−3) by using state-of-the-art quantum chemical methods.

Model Concepts for Uranyl Compounds. In order to understand the chemical bonding, excited states, and absorption/emission spectra of uranyl fluoride complexes in aqueous condition (Figure 1), it is convenient to refer to the axial-symmetric molecular orbitals (MOs) of bare uranyl (Figure 2). Under $D_{\infty h}$ symmetry, the U 7s, 5f, and 6d atomic orbitals (AOs) are split into ($s\sigma$), ($f\sigma$, $f\pi$, $f\delta$, $f\phi$), and ($d\sigma$, $d\pi$, $d\delta$) manifolds, respectively. The oxygen 2p lone-pair shells yield group orbitals of dative σ_u, σ_g, and pairs of π_u and π_g

Received: March 24, 2014
Published: June 26, 2014

dx.doi.org/10.1021/ic5006852 | Inorg. Chem. 2014, 53, 7340−7350

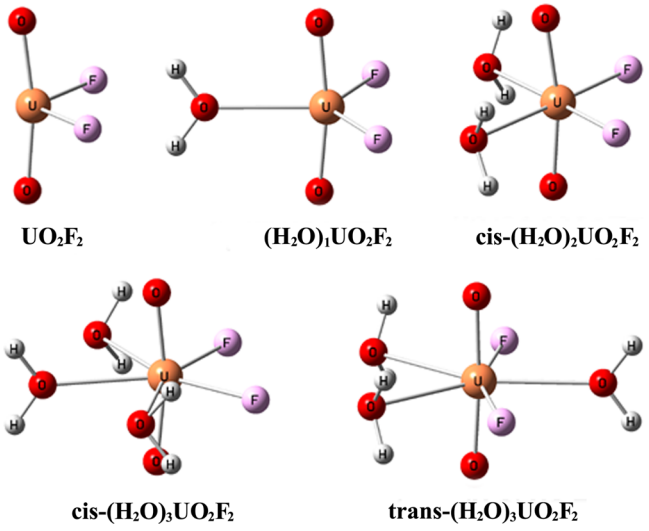

Figure 1. Optimized structures of UO_2F_2, $(H_2O)_1UO_2F_2$, *cis*-$(H_2O)_2UO_2F_2$, *cis*-$(H_2O)_3UO_2F_2$, and *trans*-$(H_2O)_3UO_2F_2$.

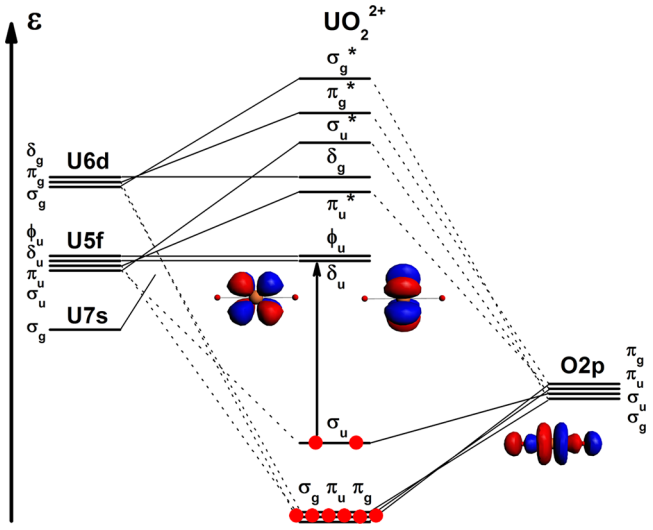

Figure 2. Qualitative scalar-relativistic valence-orbital energy level schemes for U and O atoms on the left and right sides, and $D_{\infty h}$-uranyl in the middle. The connecting lines depict major (solid line) and minor (dotted line) AO components of the molecular orbitals. The vertical arrow indicates the lowest electronic excitations between the bonding σ_u and the nonbonding U-5f δ_u and ϕ_u (see their orbital envelopes).

bonding type, which are stabilized by the U 5fσ_u,π_u and U 6dσ_g,π_g AOs, respectively. On the other hand, the U 5f and 6d AOs of σ- and π-type mix with each other into several MOs, thereby being of some antibonding character (fσ_u*, fπ_u*, dσ_g*, dπ_g*).[16] Basically, the U 7s AO does not participate in the bonding of high-valent uranium, that is, U(VI), because it is energetically pushed too high by oxygen. Among the bonding MOs, σ_u is the least stabilized one due to the well-known "push-from-below" orbital interaction of the U 6pσ_u semicore AO.[17] The localized U 5fδ_u,ϕ_u and 6dδ_g type MOs are of nonbonding character and are labeled using AO notation.

The ground states of the uranyl difluoride and its solvated complexes have a closed electronic shell and are labeled as $^1\Sigma_g^+$ in $D_{\infty h}$ symmetry. We are interested in the lowest energy excitations and de-excitations, corresponding to electronic transitions from the bonding σ_u to nonbonding ϕ_u, δ_u MOs (arrow in Figure 2), giving rise to $^{1,3}\Delta_g$ and $^{1,3}\Phi_g$ states, and vice versa for de-excitations. With the inclusion of SO-coupling, uranyl $^3\Delta_g$ splits into Π_g, Δ_g, and Φ_g, (Ω = 1_g, 2_g, 3_g), and $^3\Phi_g$ splits into Δ_g, Φ_g, and Γ_g (Ω = 2_g, 3_g, 4_g). These states are responsible for luminescence and photocatalytic features of uranyl compounds.[18]

Known Uranyl Fluoride Complexes. It is well-known that the reaction of atmospheric water with leaked UF_6 produces a series of uranyl fluoride complexes, among which UO_2F_2 is the primary uranium species.[19] The study of luminescence of UO_2F_2 is fascinating, because the luminescence of UO_2F_2 is exploited to detect UF_6 leaking with high sensitivity and rapidity.[20] In addition, the enhancement of uranyl luminescence in aqueous solution via fluoride complexation has been explored for a long time, and the uranyl fluoride species (i.e., UO_2F_2, $UO_2F_3^-$, and $UO_2F_4^{2-}$) were proposed to account for the uranyl luminescence properties (e.g., lifetime).[21] The speciation of uranyl with fluoride in the acidic aqueous solution at different temperatures were studied by TRLIF, and the individual luminescence spectra of UO_2F^+ and UO_2F_2 species at 22 and 60 °C were obtained.[5] EXAFS results show the structural information on uranyl fluoride complexes UO_2F^+, UO_2F_2, $UO_2F_3^-$, and $UO_2F_4^{2-}$ in acidic aqueous solution as follows: equatorial coordination number is around 5; U−O_{yl} distance is at 1.76−1.80 Å; U−F distance is in the range of 2.24−2.29 Å; and U−OH_2 distance is between 2.41−2.52 Å.[22−24] Besides, the stability constants of uranyl fluoride complexes UO_2F^+, UO_2F_2(aq), $UO_2F_3^-$, and $UO_2F_4^{2-}$ at a series of temperature between 25 and 70 °C were determined by spectrophotometry, and the enthalpy of complexation at 25 °C was obtained by microcalorimetry.[24]

Theoretically, the electronic spectra of isolated and hydrated UO_2F_2 were studied by Wang and Pitzer[25] on the basis of SO-MRCI calculations. The luminescent states were confirmed as the Π_g (SO term) state with a nearly pure $^3\Delta_g$ component for all compounds. They also determined and compared effects of axial and equatorial ligands on the splitting of the electronic states and concluded that splitting due to equatorial−ligand interaction is in a range of a few wavenumbers to a few thousand wavenumbers with an order of 10^1 cm^{-1} for the luminescent state. Ruipérez and Wahlgren[26] studied the electronic spectra of $UO_2F_4^{2-}$ using the SO-CASPT2 method, and they did not find the fluoride-to-uranyl charge transfer excitations at energies below 50 000 cm^{-1}. Interestingly, excited-state calculation results show that the transition of $\sigma_u \rightarrow \phi_u$ is well above those of $\sigma_u \rightarrow \delta_u$,$\pi_u$*, and it was demonstrated that the 5fϕ_u orbital is strongly pushed up in energy by the four equatorial F^- ligands relative to δ_u and π_u* orbital.[26] Detailed DFT studies have also been reported on the structural properties and electronic structures of uranyl fluorides in the gas phase and aqueous phase.[22,27−30]

2. EXPERIMENTAL AND THEORETICAL METHODS

2.1. Time-Resolved Luminescence Spectroscopy. The time-resolved luminescence spectra were recorded by excitation at 415 nm using the frequency-doubled output of a Spectra-Physics Nd:YAG laser pumped Lasertechnik-GWU MOPO laser at both 298 and 6 ± 1 K (near-liquid-helium temperature).[6] The emitted light was collected at 85° to the excitation beam and detected with a thermoelectrically cooled Princeton Instruments PIMAX intensified CCD camera after spectral dispersion through an Acton SpectroPro 300i double monochromator spectrograph. The aqueous sample (~3.5 mL) was placed in a 10 mm × 10 mm × 40 mm fused quartz cuvette fitted with

dx.doi.org/10.1021/ic5006852 | Inorg. Chem. 2014, 53, 7340−7350

a Teflon stopper. For measurement at 6 K, 50 μL of the aqueous sample solution was pipetted into a 2 mm × 4 mm × 25 mm fused quartz cuvette, and the cuvette was capped with a silicone stopper and further sealed by wrapping the cuvette inlet with paraffin. The sample cuvette was then attached to the coldfinger of a Cryo Industries RC-152 cryogenic workstation, in which the sample cuvette was directly exposed to helium vapor. The spectra were analyzed using the commercial software, IGOR, from Wavematrix, Inc.

Sample Preparation. The uranyl fluoride aqueous solution was prepared by mixing calculated volumes of stock solutions of uranyl perchlorate (pH 1, 0.01 M) with sodium fluoride solution (1 M) in 0.1 M $NaClO_4$ in a 20 mL glass vial resulting in a final uranyl concentration of 3.6×10^{-5} M and fluoride concentration of 2.2 mM at pH 3.0. The solution pH was adjusted with minute volumes of NaOH (0.5 M) and $NaClO_4$ (0.5 M). These solution conditions were selected on the basis of the results of equilibrium calculation with the MINTEQA2[31] software with the most current, critically reviewed thermodynamic stability constants for the U(VI) complexes.[32] Under these conditions, a large majority of uranyl in the solution exists as UO_2F_2 (~80%), whereas UO_2F^+ and $UO_2F_3^-$ each accounts for ~10% of the remaining UO_2^{2+}.

2.2. Computational Details. Structures and spectra of free UO_2F_2 in vacuum and its solvated complexes in aqueous solution were investigated by using WFT approaches CASPT2 and CCSD(T), without and with the SO-coupling effect, as implemented in the MOLPRO 2008.1 program.[33]

Stuttgart energy-consistent pseudopotentials (RECPs) were applied for F (the scalar ECP2MWB ones with $1s^2$ cores, optimizing the 2s2p valence shells)[34] and for U (the scalar and SO-coupled ECP60MWB ones with $1s^2-4f^{14}$ core, optimizing the 5spdf, 6spd and 7sp semicore and valence shells).[35−37] For UO_2F_2, we applied the 6-311+G* basis for O,[38] and the ECP2MWB for F with an additional d-polarization function (ζ = 0.75),[34] and ECP60MWB-SEG bases for U.[36,37] The atomic core−shells including U-5spd were not correlated. To reduce the computational cost for $(H_2O)_nUO_2F_2$ (n = 1−3), we applied the smaller basis set 6-31G* for O,[39] the basis set 6-31G** for H[40] in H_2O, and the same basis sets and RECPs as above for UO_2F_2 part. Because solvation treatment in a polarizable continuum modeling bulk water is found to have little influence on the U−O and U−F bond lengths of uranyl fluorides,[29,30] as well as the excited states of actinyl complexes,[41,42] we therefore did not include solvation effects beyond the first coordination shell in this work. A thorough investigation of such secondary solvation effect on the uranyl excited states requires accurate determination of the second or even higher solvation shells through approaches such as molecular dynamics.

Geometries and Frequencies. Geometric optimizations of the electronic *ground* states of UO_2F_2 in C_{2v} symmetry with CASPT2 and CCSD(T) were converged to gradients less than 1.0×10^{-4}. Given our aim at the influence of the number of coordination water on the luminescent properties of UO_2F_2 and the feasible computational cost, the ground-state and excited-state geometries of various $(H_2O)_nUO_2F_2$ (n = 1−3) complexes were restricted to have C_{2v} symmetry. The ground states of these complexes were optimized initially at the DFT level using LDA functional implemented in the MOLPRO 2008.1 program,[33] followed by a constraint geometry optimization at CCSD(T) level with the U and H_2O position fixed to save time. Such a two-step optimization scheme was labeled as CCSD(T)//LDA, where the geometric optimizations were converged to gradients less than 1.0×10^{-4}.

Born−Oppenheimer (BO) potential energy curves of the SO-averaged and SO-coupled *excited* electronic states versus the U−O distances were at first scanned in steps of 1 pm, with the other geometric parameters fixed at their ground-state values. The expansions of the U−O distances in the excited states were obtained from polynomial interpolation. For the lowest excited state (i.e., luminescent state), the equilibrium values of the other geometric parameters were then similarly approximated, keeping the U−O distance of the state fixed. Thereby, the approximate U−O equilibrium distances, vertical and adiabatic excitation energies, and O−U−O symmetric stretching frequencies were determined. The error of this approximation applied to the ground state has proved to be less than 4 cm^{-1}.

Electronic States. For simplicity, we use approximate $D_{\infty h}$ symmetry notations for orbitals and states of all species, except where explicitly noted otherwise. The relations between $D_{\infty h}$ and C_{2v} (UO_2F_2, $(H_2O)_{1,2,3}UO_2F_2$) symmetry species are given in Table 1.

Table 1. Correlation of Symmetry Species of Point Groups $D_{\infty h}$ and C_{2v}

$D_{\infty h}$	C_{2v}
Σ_g^+	A_1
Σ_u^+	B_1
Π_g, Δ_u, Φ_g	$A_2 + B_1$
Π_u, Δ_g, Φ_u	$A_1 + B_2$

RASSCF/CASPT2/SO Calculations. The active spaces for *ground* state CASSCF calculations of all molecular species were confined to the UO_2^{2+} moiety: The six bonding and six antibonding (*) MOs of σ_g, σ_u, π_g and π_u type from the U-5f,6d and two O-2p shells with 12 valence electrons were correlated by an active space of CAS(12,12). The active spaces for the *excited* states contained, in addition, nonbonding U-5f type orbitals of δ_u or ϕ_u symmetry (Figure 2), giving 12 electrons in 14 orbitals for $D_{\infty h}$-UO_2^{2+}, CAS(12,14),[13] or 12 electrons in 13 orbitals for C_{2v}-UO_2F_2 and C_{2v}-$(H_2O)_{1,2,3}UO_2F_2$, CAS(12,13). In the equatorially ligated uranyl species, the degeneracies of δ_u and ϕ_u are both lifted, with little orbital and configuration mixing, as known from the literature.[43] Large CAS-(12,16) calculations with both δ_u or ϕ_u pairs simultaneously in the active space were deemed unnecessary.

SO-averaged (i.e., spin−orbit-free) CASPT2 calculations were performed on the ground states, and on all excited states arising from single excitations out of the σ_u HOMO into the nonbonding orbitals of U-5fδ_u,ϕ_u type, which gives four singlets and four triplets. Individually optimized CASSCF orbitals were used for each state, except for the singlet excited states of the same symmetry as the ground state. Here, the ground-state orbitals facilitate converging to correct occupation schemes. A level shift of 0.3 au was applied to improve the CASPT2 convergence.[44,45]

Because of the near-degeneracy of some excited states of UO_2F_2, the application of g_1-corrected CAS Fock-operators was not always feasible. Therefore, the g_1 corrections of respective states of UO_2^{2+} in our previously published paper of UO_2Cl_2 were added to the uncorrected values of the states of UO_2F_2,[13] as suggested by Pierloot (designated as g_1').[43]

SO coupling was treated by a restricted RAS-SI/SO approach[46,47] in an active space of the mentioned 16 orbitals, labeled RAS(12,16). Up to four electrons were excited into 10 virtual occupied orbitals (i.e., six antibonding orbitals and four nonbonding orbitals) for UO_2F_2, whereas such an electron restriction scheme, labeled as **S1**, is not feasible for $(H_2O)_{1,2,3}UO_2F_2$ due to the intruder of higher excited states. Therefore, a new restriction scheme, labeled as **S2**, in which up to one electron was excited into four nonbonding orbitals and four electrons into six antibonding orbitals was used in SO calculations of $(H_2O)_{1,2,3}UO_2F_2$, as well as UO_2F_2 for the sake of comparison. The SO-averaged RASSCF singlet and triplet wave functions were determined on the basis of state-averaged (SA) RASSCF orbitals of the ground and all excited singlet states. The resulting RASSCF wave functions were then used to construct a 17 × 17 SO coupling matrix, where the diagonal elements were correlation-corrected by using the CASPT2 energies. Single-point SA-CASSCF test calculations with CAS(12,16) confirmed that the errors in **S1** scheme remain less than 64 cm^{-1} and in **S2** scheme, less than 54 cm^{-1}, respectively, for UO_2F_2. This combination of RASSCF/SI-SO with CASPT2 is labeled as RASSCF/CASPT2/SO.

RASSCF/CCSD(T)/SO Calculations. We also applied a RASSCF/CCSD(T)/SO approach[48,49] that has been used in the study of UO_2Cl_2 in Ar matrix[13] to the excited states of UO_2F_2 and $(H_2O)_{1,2,3}UO_2F_2$ with the same techniques. The SO-averaged

dx.doi.org/10.1021/ic5006852 | Inorg. Chem. 2014, 53, 7340−7350

CCSD(T) calculations were performed for the ground and four excited triplet state energy curves at first. Then in order to approximately obtain the CCSD(T) energy curves of excited singlet states at the SO-averaged level, the CASPT2 energy difference between the excited singlet and triplet pair was calculated and added ad hoc to the corresponding CCSD(T) energy of the excited triplet state pointwise. The SO-coupling effect was included in the same way as that in the RASSCF/CASPT2/SO calculations but with the diagonal elements corrected by the CCSD(T) state energies.

Simulation of Luminescent Spectra and Normal Coordinates Analysis. As outlined in our previous work of UO_2Cl_2,[13] we used Franck−Condon formulas of Fonger and Struck[50] to simulate the luminescence spectra of UO_2F_2 in gas phase and in solution. Ground-state geometry optimizations and vibrational frequency calculations of UO_2F_2 were performed with DFT/PBE using Gaussian 03[51] with the same basis sets as in the CASPT2 and CCSD(T) calculations above. The Wilson−Decius FG method[52] and the McIntosh and Peterson's program[53] for producing F and G matrix were used, and the dimensionless geometric displacement parameter upon electronic transition for O−U−O, Δ, and the Huang−Rhys factor,[54] *S*, were obtained.

3. EXPERIMENTAL RESULTS

The UO_2F_2 solution displayed moderately intense luminescence spectra with well-resolved vibronic bands located at 498.1, 520.2, 544.1, 569.3, and 598.4 nm at near liquid helium temperature and 499.0, 521.4, 545.2, 570.9, and 599.3 nm at room temperature. These spectral features were characteristic of uranyl complexes,[1,6,55] and the observed vibronic peak positions were consistent with those reported by others under different solution conditions where UO_2F_2 was the dominant species.[5,21f] The present vibronic band spacing of 849 cm^{-1} closely matched the value obtained by Beitz and Williams.[21f]

4. COMPUTATIONAL RESULTS AND DISCUSSION

CASPT2 and CCSD(T) Results of UO_2F_2. *Optimized Structure of UO_2F_2.* As shown in Table 2, the optimized ground-state geometries of UO_2F_2 from CASPT2 and CCSD(T) are consistent, both indicating the multiple U−O and dative U−F bonding. CCSD(T) gives ∼0.5 pm shorter U−O distance while ∼0.5 pm longer U−F distance than CASPT2. The bending of the linear OUO unit by ∼11° can be rationalized in terms of 5f-6d-7s hybridization or electrostatic F^{-}-O^{2-} repulsion or valence-shell electron-pair repulsion. The lowest excited states of UO_2F_2 correspond to $\sigma_u \rightarrow \delta_u,\phi_u$ transitions (Figure 2), similar to those in other uranyl compounds.,[12,13,26,43,56−58] The U−O bond lengths of the triplet SO-averaged states are expanded by 5.9 to 8.3 pm, whereas the U−F bond lengths vary by less than 2.1 pm. The OUO and FUF angles are reduced by 0.8 up to 12.6°, except the FUF angle of $^3B_2(^3\Delta_g)$ state, which increases by 0.7°. Obviously, the $^3\Phi_g$ type states have longer U−O bond length and smaller OUO angle than the $^3\Delta_g$ type ones due to the equatorial coordination of F ligands.

Table 2. Geometrical Parameters of UO_2F_2 from CASPT2 and CCSD(T) Calculations for the Ground and Four Lowest Excited Triplet States at the SO-Averaged Level

state in $C_{2v}(D_{\infty h})$	*R*(U−O)/pm	*R*(U−F)/pm	∠OUO/°	∠FUF/°
		CASPT2		
$^1A_1(^1\Sigma_g^+)$	176.22	207.63	169.5	112.9
		CCSD(T)		
$^1A_1(^1\Sigma_g^+)$	175.75	208.13	169.1	113.8
$^3A_1(^3\Delta_g)$	182.09	206.04	162.3	104.9
$^3B_2(^3\Delta_g)$	181.62	207.83	168.3	114.5
$^3B_1(^3\Phi_g)$	184.05	207.02	156.7	101.2
$^3A_2(^3\Phi_g)$	183.88	207.66	158.4	103.9

SO-Averaged Potential Energy Curves of Excited States. CASPT2 and CCSD(T) give similar energy curves of the lowest states of UO_2F_2 arising from the $\sigma_u \rightarrow \delta_u,\phi_u$ excitations at the SO-averaged level. For the sake of simplicity, SR CCSD(T) results are displayed in Figure 3.

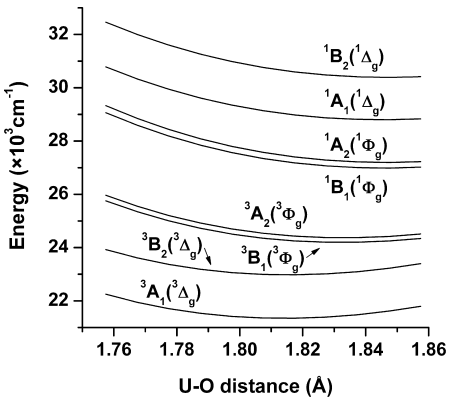

Figure 3. Energy curves of the low-lying excited states of UO_2F_2 for the O−U−O symmetric stretching at the SR level from CCSD(T) calculations.

The respective numerical spectroscopic data from SO-averaged CASPT2-[g_1'] and CCSD(T) scans and CCSD(T) full-optimization are collected in Table 3. The singlet−triplet splittings of UO_2F_2 for the Δ_g and Φ_g are 8.3 and 3.3 × 10^3 cm^{-1}, respectively. Correspondingly, the fluorine ligand splittings for these two types of states are 1.7 × 10^3 and 0.2 × 10^3 cm^{-1}. This huge difference in ligand field splitting is due to the different interaction strength between fluorine 2p with the two 5fδ_u orbitals of different symmetries, that is, strong π interaction for a_2 symmetry while no interaction for b_1 symmetry, which has been observed in other uranyl compounds as well.[13,25,43]

For the excited triplet states, the CCSD(T) scans reproduce the CCSD(T) fully optimized results quite well, within 1 pm and 741 cm^{-1} for U−O bond lengths and adiabatic excitation energies, respectively. Therefore, the CCSD(T) scans of the BO energy curves yield reasonable approximations to the CCSD(T) optimized results.

The U−O bond lengths and the O−U−O symmetric stretching frequencies ν_s of the excited states from CCSD(T) scans are consistent with CASPT2-[g_1'] results with difference within 0.2 pm and 8 cm^{-1} respectively. The excitation energies from the former are larger than the latter by 1000 up to 1600 cm^{-1}. Besides, the ν_s values of the ground state are larger by 40 cm^{-1}. Therefore, the calculation results from the two methods have noticeable differences in excitation energy and ground-state ν_s value.

SO-Coupled Results. SO-coupled energy curves of the low-lying, spin-triplet-derived excited states of UO_2F_2 along the O−U−O symmetric stretching mode are presented in Figure 4, where we only show the RASSCF/CCSD(T)/SO results. The respective numerical spectroscopic data with Ω-values from SO-coupled CASPT2-[g_1'] and CCSD(T) are collected in Table 4.

The RASSCF/CCSD(T)/SO results for UO_2F_2 are similar to the RASSCF/CASPT2-[g_1']/SO ones with respect to the order of the energy levels and to the U−O distances and ν_s values of the excited states. Their differences in excitation energies and ground-state ν_s value are also found at the SO-averaged level. The lowest three SO excited states, all of $^3\Delta_g$ type, are very close in energy with a difference within 100 cm^{-1}. The fourth lowest SO state of $^3\Phi_g$ type is some 850 cm^{-1} higher, which is close to the energy level of O−U−O symmetric stretching vibration and is likely to contribute to the hot band in the luminescence spectra at room temperature as found in uranyl−glycine−water complexes.[12]

Despite the similarity of UO_2F_2 and UO_2Cl_2, their luminescent-state characters are different. The luminescent-state is $^3\Delta_g$ type for UO_2F_2 and $^3\Phi_g$ type for UO_2Cl_2. This difference is determined by the competition of SO coupling and the ligand field effect, where the former more stabilizes the $^3\Phi_g$ state and the latter more stabilizes the $^3\Delta_g$ state due to different coordination abilities of F and Cl. The weak chlorine ligand field gives the energy gap of around 1800 cm^{-1}

dx.doi.org/10.1021/ic5006852 | Inorg. Chem. 2014, 53, 7340−7350

Table 3. Spectroscopic Data from SO-Averaged CASPT2-[g_1'] and CCSD(T) Scan Calculations (CCSD(T) Optimized Results in Parentheses) for UO_2F_2

$C_{2v}(D_{\infty h})$	E^a/cm^{-1}	$R_e{}^b$/pm	$T_e{}^c$/cm^{-1}	$\nu_s{}^d$/cm^{-1}	E^a/cm^{-1}	$R_e{}^b$/pm	T_e/cm^{-1}	$\nu_s{}^d$/cm^{-1}
	CASPT2-[g_1']				CCSD(T)			
$X^1A_1(X^1\Sigma_g^+)$		176.20	0	851		175.75		891[e]
$a^3A_1(^3\Delta_g)$	20 968	181.34	20 207	747	22 250	181.53 (182.09)	21 340 (20 910)	750
$a^3B_2(^3\Delta_g)$	22 620	181.50	21 815	746	23 924	181.67 (181.62)	22 968 (22 968)	751
$a^3B_1(^3\Phi_g)$	24 575	183.15	23 176	761	25 755	183.22 (184.05)	24 181 (23 440)	766
$a^3A_2(^3\Phi_g)$	24 760	183.19	23 337	763	25 964	183.28 (183.88)	24 358 (23 762)	768
$a^1B_1(^1\Phi_g)$	27 863	184.41	25 928	759	29 064	184.35	26 980	767
$a^1A_2(^1\Phi_g)$	28 101	184.49	26 122	761	29 328	184.43	27 190	769
$a^1A_1(^1\Delta_g)$	29 168	184.36	27 331	746	30 782	184.33	28 793	751
$a^1B_2(^1\Delta_g)$	30 826	184.56	28 895	748	32 461	184.49	30 383	754

[a]Vertical excitation energy E at ground-state geometry. [b]U−O equilibrium distance R_e. [c]Calculated adiabatic excitation energy T_e without zero-point vibrational energy corrections. [d]O−U−O symmetric stretching frequency ν_s. [e]From the ground-state frequency calculation.

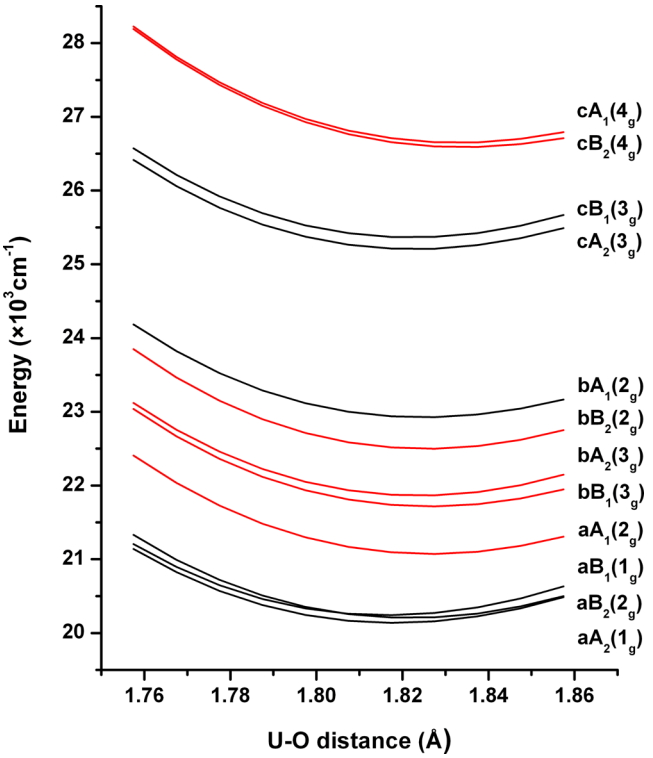

Figure 4. Energy curves of excited states of UO_2F_2 along the O−U−O symmetric stretching coordinate from RASSCF/CCSD(T)/SO calculations (red curves: $^3\Phi$ type; black curves: $^3\Delta$ type). The Ω-values are listed in the parentheses after the double-group state symbols.

between the lower $^3\Phi_g$ state and the lower $^3\Delta_g$ state at SR level in the UO_2Cl_2,[13] whereas the stronger fluorine ligand field with significant U−F π-interaction gives a nearly doubled value of 3500 cm^{-1}. According to SO-CASPT2 vertical excitation energies of $UO_2{}^{2+}$, the energy lowering of the lowest SO-splitting term of $^3\Phi_g$ (i.e., 2_g) relative to its SR parent (i.e., $^3\Phi_g$) is around 3400 cm^{-1}, although the corresponding SO stabilization energy for the $^3\Delta_g$ state is around 1560 cm^{-1} (i.e., 1_g relative to the $^3\Delta_g$). [13] Therefore, the strong SO stabilization of $^3\Phi_g$ surpasses the weak destabilization from the ligand field, resulting in the dominated $^3\Phi_g$ character of luminescent state in UO_2Cl_2. The situation is vice versa for the dominated $^3\Delta_g$ character in UO_2F_2. The energy gap of 1800 cm^{-1} between the lower $^3\Phi_g$ and $^3\Delta_g$ at the SR level can be used as a threshold to judge the luminescent-state character. For example, from UO_2Cl_2 to $UO_2Cl_3{}^-$ and further to $UO_2Cl_4{}^{2-}$, more Cl^- coordination gives rise to the change of luminescent-state character from $^3\Phi_g$ to $^3\Delta_g$ due to the large energy gap of around 4000 cm^{-1} in the latter.

Literature results on the vertical excitation energies of UO_2F_2 from previous SO-MRCI calculations are also displayed in Table 4. The ordering of the energy levels are consistent between our RASSCF/CCSD(T)/SO results and the SO-MRCI results, except the aB_2 state ($^3\Delta_g$ type), although excitation energies moderately differ due to different active spaces and atomic basis sets. Generally, the energy differences decrease from 2.5 × 10^3 to 0.9 × 10^3 cm^{-1} as the energy level increases. The similar case is found in the comparison of our RASSCF/CASPT2-[g_1']/SO results with the SO-MRCI results, although the former is closer to the latter compared to the CCSD(T) results.

Simulation of Luminescence Spectrum in Gas Phase. The totally symmetric breathing modes are usually reflected in vibronic progressions of symmetric molecules, which can be used to estimate the bond length changes when including a topological mass factor.[59] For UO_2F_2, the three spectroscopically most important symmetric vibrational modes are specified in Table 5. Their characters are O−U−O stretching, F−U−F stretching, and a mix of O−U−O and O−U−F bending, respectively. The other symmetric vibration (i.e., the F−U−F bending mode) is found to contribute insignificantly to the shape of the spectra due to the small frequency.

All numerical parameters for the spectral simulations from both CASPT2-[g_1'] and CCSD(T) are listed in Table 6, and correspondingly, the simulated spectra are shown in Figure 5, where the energy origin is set the same (i.e. both from CCSD(T) results). These two methods give similar simulation results, where the luminescence spectrum is dominated by a progression of the symmetric O−U−O stretching vibration of ~870 cm^{-1} of the electronic ground state. Each band has two weak side bands. The first one is lower by 560 cm^{-1}, corresponding to F−U−F stretching, while the second one is the tails of the vibrational progression of O−U−O bending mode with a vibration frequency of ~200 cm^{-1}. However, the relative intensity distributions of the first two modes are different between these two simulation results due to the slightly larger geometrical changes (Δ) from CCSD(T) than from CASPT2-[g_1'].

Influence of H_2O Coordination. *Ground-State Structures of $(H_2O)_nUO_2F_2$.* In aqueous solution, water molecules as weak Lewis bases can coordinate to uranyl in the equatorial plane to saturate the coordination shell. We simulate the water coordination effect by $(H_2O)_nUO_2F_2$ (n = 1−3) complexes, neglecting solvent effects beyond the first coordination shell. Given that five coordination in the equatorial plane dominates in common uranyl complexes, the case of n > 3 is not considered here.

The ground-state structures of $(H_2O)_nUO_2F_2$ (n = 1−3) with constraint of C_{2v} symmetry were optimized at CCSD(T)//LDA level. For n = 2, we choose the energetically more stable *cis* structure[29] to study the influencing trend of H_2O coordination on luminescence. For n = 3, both *cis* and *trans* structures are included. The optimized structures of $(H_2O)_nUO_2F_2$ (n = 1−3) are chosen to simulate the

dx.doi.org/10.1021/ic5006852 | Inorg. Chem. 2014, 53, 7340−7350

Table 4. Spectroscopic Data from SO-Coupled CASPT2-[g_1'] and CCSD(T) for UO_2F_2[a]

state (Ω)	main	E/cm^{-1}	R_e/pm	T_e/cm^{-1}	ν_s/cm^{-1}	E/cm^{-1}	R_e/pm	T_e/cm^{-1}	ν_s/cm^{-1}	E/cm^{-1}
		CASPT2-[g_1']				CCSD(T)				ref 25
$XA_1(0_g)$			176.20		851		175.75		891	
$aA_2(1_g)$	$^3\Delta_g$	19 857	181.73	19 012	736	21 141	181.94	20 128	739	18 628
$aB_2(2_g)$	$^3\Delta_g$	20 054	182.05	19 093	743	21 330	182.26	20 195	746	18 967
$aB_1(1_g)$	$^3\Delta_g$	19 920	181.58	19 106	742	21 207	181.77	20 233	745	18 652
$aA_1(2_g)$	$^3\Phi_g$	21 138	182.56	20 005	756	22 407	182.70	21 062	762	20 465
$bB_1(3_g)$	$^3\Phi_g$	21 793	182.56	20 619	754	23 038	182.69	21 706	759	21 176
$bA_2(3_g)$	$^3\Phi_g$	21 878	182.33	20 757	763	23 121	182.44	21 853	768	21 278
$bB_2(2_g)$	$^3\Phi_g$	22 631	182.55	21 420	771	23 850	182.61	22 486	777	22 626
$bA_1(2_g)$	$^3\Delta_g$	22 894	182.46	21 788	751	24 186	182.56	22 912	755	22 838
$cA_2(3_g)$	$^3\Delta_g$	25 174	182.26	24 117	758	26 417	182.36	25 193	762	25 100
$cB_1(3_g)$	$^3\Delta_g$	25 319	182.20	24 266	764	26 573	182.30	25 354	767	25 031
$cB_2(4_g)$	$^3\Phi_g$	26 997	183.30	25 562	753	28 191	183.38	26 574	760	27 284
$cA_1(4_g)$	$^3\Phi_g$	27 028	183.18	25 617	759	28 224	183.26	26 636	766	27 281

[a]See footnotes of Table 3.

Table 5. Vibrational Normal Mode Coordinates of OUO Symmetric Stretching s(OUO) and Bending b(OUO) and That of FUF Symmetric Stretching s(FUF) in UO_2F_2, from DFT/PBE Frequency Calculations

internal coordinates	normal coordinate (unit: (g/mol)$^{1/2}$)		
(unit: Å or Å × rad)	s(OUO)	s(FUF)	b(OUO)
$R(U_1-O_2)$	−2.79	0.44	0.04
$R(U_1-O_3)$	−2.79	0.44	0.04
$R(U_1-F_4)$	−0.49	−2.95	0.41
$R(U_1-F_5)$	−0.49	−2.95	0.41
$\angle(O_2-U_1-O_3)$	−0.13	−0.16	−3.55
$\angle(O_2-U_1-F_4)$	0.04	0.04	0.96
$\angle(O_2-U_1-F_5)$	0.04	0.04	0.96
$\angle(O_3-U_1-F_4)$	0.04	0.04	0.96
$\angle(O_3-U_1-F_5)$	0.04	0.04	0.96
$\angle(F_4-U_1-F_5)$	0.00	0.15	1.01

Table 6. Parameters for Simulation of Luminescence Spectra of UO_2F_2

parameter[a]	CASPT2-[g_1']	CCSD(T)
ΔR(U−O)/Å	0.0553	0.0619
ΔR(U−F)/Å	−0.0134	−0.0137
$\Delta(\angle$OUO)/°	−4.86	−6.96
$\Delta(\angle$FUF)/°	−6.63	−7.46
$\Delta(\angle$OUF)/°	1.70	2.36
$\nu_{s,g}$(OUO)/cm^{-1}	851	891[c]
$\nu_{s,e}$(OUO)/cm^{-1}	736	739
$\nu_{s,g}$(FUF)/cm^{-1}	557[b]	563[c]
$\nu_{b,g}$(OUO)/cm^{-1}	193[b]	213[c]
ΔQ_{s_O}/Å·(g/mol)$^{1/2}$	0.28	0.31
ΔQ_{s_F}/Å·(g/mol)$^{1/2}$	0.13	0.14
ΔQ_b/Å·(g/mol)$^{1/2}$	0.29	0.45
E_{00}/cm^{-1}	18 955	20 051

[a]Changes of geometrical parameters between the ground and luminescent state; $\nu_{s,g}$ and $\nu_{b,g}$ are the symmetric stretching and bending frequencies of the ground state; $\nu_{s,e}$ is the stretching frequency of the luminescent state; ΔQ_s and ΔQ_b are the corresponding normal coordinate displacements; E_{00} is adiabatic excitation energy with inclusion of zero-point vibrational energy corrections, and only the vibrational frequency change of the O−U−O symmetric stretching is considered. [b]From DFT/PBE calculations. [c]From ground-state frequency calculations.

water coordination effects and are displayed in Figure 1. The corresponding geometrical parameters are summarized in Table 7, where the UO_2F_2 geometrical parameters are also included for comparison.

The U−OH_2 distances of 2.39−2.55 Å show typical dative bond of $H_2O \rightarrow UO_2F_2$, consistent with experimental EXAFS results of 2.41−2.52 Å in uranyl fluoride aqueous solution.[22−24] Equatorial coordination of H_2O molecules expands the U−O distances and U−F distances by around 0.9 and 2.6 pm per H_2O, respectively. This scenario is in contrast to the negligible influence on bond length from Ar coordination to UO_2Cl_2, showing a much stronger interaction of H_2O with UO_2F_2. The O−U−O bending angle due to the F ligands is slightly alleviated by H_2O molecule coordination in *trans* position. Compared to UO_2F_2, the F−U−F angle is reduced by about 24° in *cis*-$(H_2O)_3UO_2F_2$ but greatly widened by 41° in *trans*-$(H_2O)_3UO_2F_2$.

SO-Averaged Excited States of $(H_2O)_nUO_2F_2$. In general, because the CCSD(T) method treats dynamic electron correlation more accurately, it gives better excitation energies than CASPT2-[g_1'] method for low-lying triplet excited states with single reference character,[13] which are mainly responsible for luminescence and low-energy absorption spectra. Therefore, only the CCSD(T) method is used to calculate the excited states of $(H_2O)_nUO_2F_2$. The corresponding numerical spectroscopic data are displayed in Table 8. The electronic excitation patterns of these five species including the bare UO_2F_2 in Table 3 are quite similar. The water solvent environment increases the first adiabatic excitation energy by a few 100 cm^{-1} up to 2.2 × 10^3 cm^{-1} in *trans*-$(H_2O)_3UO_2F_2$. The energy difference between the lower $^3\Phi_g$ -type state and the lower $^3\Delta_g$-type state increases around 500 cm^{-1} per H_2O coordination, indicating the increasing destabilization of Φ_g state due to ligand field repulsion. Besides, equatorial coordination of H_2O molecules expands the U−O distances of the excited states by around 1.4 pm per H_2O. Correspondingly, the O−U−O symmetric stretching frequencies ν_s decrease by 14 cm^{-1} per H_2O. These changes above indicate that H_2O-coordination significantly affects excited-state properties of these uranyl complexes.

SO-Coupled Excited States of $(H_2O)_nUO_2F_2$. RASSCF/CCSD(T)/SO-calculated numerical spectroscopic data are summarized in Tables 9, 10, and 11 for the cases of n = 0−1-, 2-, and 3-coordinated H_2O molecules, respectively. In the $(H_2O)_nUO_2F_2$ (n = 1−3), the energy levels of excited states display two types of distributions. The first type occurs in the n = 0 and 1, where the lowest three SO states are all of $^3\Delta_g$ character and the fourth one is of $^3\Phi_g$ character. Although the second type occurring in the n = 2 and 3 is that the lowest six SO states are all of $^3\Delta_g$ character and the highest six ones are all of $^3\Phi_g$ character. The transition from the first to the second type distribution happens in n = 2, where the components of $^3\Delta_g$ and $^3\Phi_g$ are almost the

dx.doi.org/10.1021/ic5006852 | Inorg. Chem. 2014, 53, 7340−7350

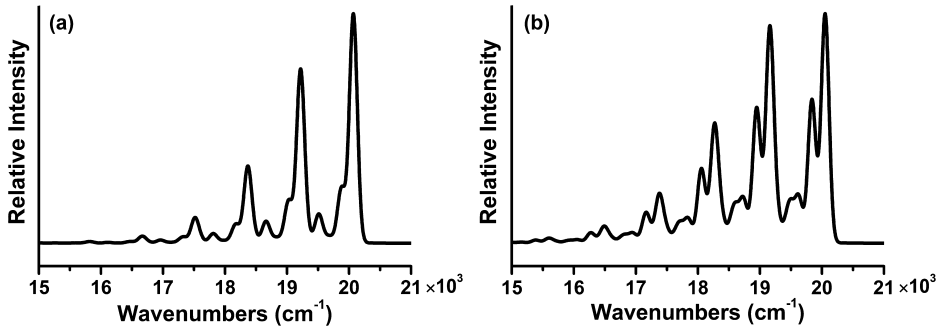

Figure 5. Theoretically predicted luminescence spectra of gas-phase UO_2F_2 with bandwidth of 63 cm^{-1}: (a) RASSCF/CASPT2-[g_1']/SO and (b) RASSCF/CCSD(T)/SO.

Table 7. Ground-State Geometrical Parameters of $(H_2O)_nUO_2F_2$ (n = 1−3) from CCSD(T)//LDA Calculations at the SO-Averaged Level[a]

compds	R(U−O_{ax})[b]/pm	R(U−F)/pm	∠OUO/°	∠FUF/°	R(U−O_{w1})[c]/pm	R(U−O_{w2})[c]/pm
UO_2F_2	175.75	208.13	169.1	113.8		
$(H_2O)_1UO_2F_2$	176.79	210.51	170.6	124.5	239.24	
cis-$(H_2O)_2UO_2F_2$	177.67	213.07	169.3	107.3	245.91	
cis-$(H_2O)_3UO_2F_2$	178.16	215.18	169.4	90.1	242.88	254.67
trans-$(H_2O)_3UO_2F_2$	177.74	217.41	175.9	155.1	242.23	250.89

[a]Ground-state geometrical parameters of UO_2F_2 are from CCSD(T) calculations. [b]Bond length of U and axial O. [c]Bond length of U ← OH_2.

Table 8. Spectroscopic Data from SO-Averaged CCSD(T) for $(H_2O)_nUO_2F_2$ (n = 1−3)[a]

	E/cm^{-1}	R_e/pm	T_e/cm^{-1}	ν_s/cm^{-1}	E/cm^{-1}	R_e/pm	T_e/cm^{-1}	ν_s/cm^{-1}
$C_{2v}(D_{\infty h})$	$(H_2O)_1UO_2F_2$				*cis*-$(H_2O)_2UO_2F_2$			
$X^1A_1(X^1\Sigma_g^+)$		176.79		868		177.67		854
$a^3A_1(^3\Delta_g)$	23 051	182.86	22 070	745	22 741	184.02	21 703	733
$a^3B_2(^3\Delta_g)$	24 081	182.99	23 055	746	24 506	184.08	23 445	734
$a^3B_1(^3\Phi_g)$	26 839	184.71	25 165	745	28 759	186.21	26 904	727
$a^3A_2(^3\Phi_g)$	27 454	184.90	25 689	748	27 701	186.11	25 878	729
$a^1B_1(^1\Phi_g)$	30 277	185.94	28 074	740	32 044	187.56	29 604	719
$a^1A_2(^1\Phi_g)$	30 948	186.17	28 607	745	31 138	187.53	28 170	720
$a^1A_1(^1\Delta_g)$	31 458	187.19	28 844	717	30 919	188.45	28 157	703
$a^1B_2(^1\Delta_g)$	32 669	185.99	30 508	730	32 946	187.38	30 679	706
	cis-$(H_2O)_3UO_2F_2$				*trans*-$(H_2O)_3UO_2F_2$			
$X^1A_1(X^1\Sigma_g^+)$		178.16		845		177.74		852
$a^3A_1(^3\Delta_g)$	22 953	184.76	21 873	718	24 700	184.39	23 586	725
$a^3B_2(^3\Delta_g)$	24 620	184.79	23 528	719	24 042	184.43	22 912	725
$a^3B_1(^3\Phi_g)$	29 554	186.78	27 685	723	29 039	186.50	27 111	722
$a^3A_2(^3\Phi_g)$	27 725	186.71	25 893	721	30 350	186.61	28 375	722
$a^1B_1(^1\Phi_g)$	30 988	188.24	30 479	716	32 662	187.78	30 126	723
$a^1A_2(^1\Phi_g)$	31 063	188.14	28 617	714	33 967	187.89	31 370	723
$a^1A_1(^1\Delta_g)$	31 009	189.21	28 152	698	33 109	188.61	30 300	704
$a^1B_2(^1\Delta_g)$	32 997	188.12	30 655	700	32 775	187.47	30 481	709

[a]See footnotes of Table 3; the ordering of excited states is arranged the same as that of UO_2F_2 in Table 3.

same in the SO states of 2_g and 3_g representation. Clearly the varying strengths of the ligand field of different numbers of water ligands account for the relative position of the $^3\Delta_g$ and $^3\Phi_g$ derived SO-states.

As the number of coordinated H_2O molecules increases, the 1_g and 2_g states of main $^3\Delta_g$ character slightly change within 1000 cm^{-1}, whereas the 3_g states of the same character descend by 2000−3000 cm^{-1}. All the SO states of $^3\Phi_g$ type are lifted up remarkably by 2000−6000 cm^{-1}. The trend of U−O distance and ν_s values of the excited states are similar to those at the SO-averaged level. Besides, for the corresponding excited states, the excitation energy differences between *cis*- and *trans*-$(H_2O)_3UO_2F_2$ are up to 1800 cm^{-1}. Our RASSCF/CCSD(T)/SO results of *trans*-$(H_2O)_3UO_2F_2$ give the same ordering of the energy levels as the SO-MRCI results by Wang and Pitzer;[25] however, as to vertical excitation energy, the former are higher than the latter by 2600−4000 cm^{-1}.

Simulation of Luminescence Spectrum in Aqueous Phase. The luminescent-state properties of $(H_2O)_nUO_2F_2$ (n = 0, 1, 2, 3) are collected in Table 12. Obviously, H_2O coordination does not change the dominance of $^3\Delta_g$ character as the luminescent state. Instead, it enhances the character due to the ligand field of water, consistent with the result that carbonyl ligand coordination to UO_2Cl_2 alters the luminescent state to be of $^3\Delta_g$ character.[56] However, the U−O bond length changes upon electronic transition, as does the O−U−O symmetric stretching vibrational frequencies υ_s of the luminescent state. Accordingly, the overall spectral shapes and the adiabatic excitation energies are appreciably modified by the H_2O ligands. At the saturation of H_2O coordination, these values are stable at 6.80 pm, 720

dx.doi.org/10.1021/ic5006852 | Inorg. Chem. 2014, 53, 7340−7350

Table 9. Spectroscopic Data from SO-Coupled CCSD(T) for UO_2F_2 and $(H_2O)_1UO_2F_2$[a]

state (Ω)	main	E/cm^{-1}	R_e/pm	T_e/cm^{-1}	ν_s/cm^{-1}	E/cm^{-1}	R_e/pm	T_e/cm^{-1}	ν_s/cm^{-1}
		UO_2F_2[b]				$(H_2O)_1UO_2F_2$			
$XA_1(0_g)$			175.75				176.79		
$aA_2(1_g)$	$^3\Delta_g$	21 164	181.80	20 179	745	21 857	183.00	20 835	744
$aB_2(2_g)$	$^3\Delta_g$	21 343	182.25	20 216	744	22 288	183.47	21 143	731
$aB_1(1_g)$	$^3\Delta_g$	21 213	181.72	20 249	747	21 875	182.96	20 862	745
$aA_1(2_g)$	$^3\Phi_g$	22 384	182.91	20 993	751	23 007	183.94	21 694	732
$bB_1(3_g)$	$^3\Phi_g$	23 032	182.81	21 673	753	23 474	184.11	22 365	733
$bA_2(3_g)$	$^3\Phi_g$	23 083	182.70	21 757	755	23 689	184.05	22 319	736
$bB_2(2_g)$	$^3\Phi_g$	23 829	182.73	22 431	773	24 860	184.43	23 276	751
$bA_1(2_g)$	$^3\Delta_g$	24 226	182.36	22 993	765	25 020	184.37	23 479	746
$cA_2(3_g)$	$^3\Delta_g$	26 432	182.28	25 226	766	27 257	183.84	25 894	755
$cB_1(3_g)$	$^3\Delta_g$	26 571	182.30	25 352	768	27 568	183.98	26 136	759
$cB_2(4_g)$	$^3\Phi_g$	28 211	183.26	26 624	766	29 517	184.42	27 798	745
$cA_1(4_g)$	$^3\Phi_g$	28 232	183.23	26 653	767	29 544	184.80	27 833	746

[a]See footnotes of Table 3. [b]Different from Table 4, here restriction scheme S2 in RAS-SI/SO calculation was applied in accord with $(H_2O)_nUO_2F_2$ (n = 1−3) calculations.

Table 10. Spectroscopic Data from SO-Coupled CCSD(T) for *cis*-$(H_2O)_2UO_2F_2$[a]

state (Ω)	main	E/cm^{-1}	R_e/pm	T_e/cm^{-1}	ν_s/cm^{-1}
$XA_1(0_g)$			177.67		
$aA_2(1_g)$	$^3\Delta_g$	21 631	184.41	20 500	720
$aB_1(1_g)$	$^3\Delta_g$	21 657	184.36	20 540	721
$aB_2(2_g)$	$^3\Delta_g$	21 988	184.57	20 797	722
$aA_1(2_g)$	$^3\Delta_g$	23 890	184.35	22 757	727
$bB_1(3_g)$	$^3\Delta_g$	24 348	184.72	23 081	729
$bA_2(3_g)$	$^3\Delta_g$	24 542	184.53	23 339	730
$bA_1(2_g)$	$^3\Phi_g$	25 442	186.46	23 496	724
$bB_2(2_g)$	$^3\Phi_g$	26 084	185.48	24 461	745
$cB_1(3_g)$	$^3\Phi_g$	27 909	185.30	26 373	740
$cA_2(3_g)$	$^3\Phi_g$	28 431	185.60	26 776	740
$cA_1(4_g)$	$^3\Phi_g$	30 461	186.49	28 516	721
$cB_2(4_g)$	$^3\Phi_g$	30 553	186.45	28 638	719

[a]See footnotes of Table 3.

cm^{-1}, and 21 000 cm^{-1}, respectively. In addition, the ν_s value of the ground state is stable at 850 cm^{-1}. The spectral parameters from theory deductions and experimental observations are also displayed in Table 12, and they are consistent in adiabatic excitation energy and in ground- and luminescence-state ν_s value.

Using the theoretical spectral parameters and experimental energy origin, the simulated spectra are obtained as shown in Figure 6, where the most intense band is calibrated to be consistent with the experimental result.[60] The experimental emission spectra measured at liquid helium temperature and at room temperature are very similar in that they are dominated by a progression of the O−U−O symmetric stretching vibration of 849 cm^{-1} of the electronic ground state and that the second peak at the higher energy part shows the strongest intensity. The differences are also obvious because in the room-temperature emission spectrum, a hot band with high intensity (around 11%) occurs at the high energy side and that the peak broadening is more significant than that at low temperature. The high intensity of the high-energy foot of the progression has been discussed in details in the uranyl−glycine−water system,[12] which is due to an overlay of vibrational hot bands and emission from thermally populated, electronically excited states accidentally near-degenerate with the first O−U−O vibrationally excited state. Similarly in the aquo−UO_2F_2 system, the second group of electronically excited states containing 1−2 states lies 300−860 cm^{-1} above the first group, which can be thermally populated at room temperature and contribute 3%−13% to the high energy foot if considering the same oscillator strength

Table 11. Spectroscopic Data from SO-Coupled CCSD(T) for $(H_2O)_3UO_2F_2$[a]

state (Ω)	main	E/cm^{-1}	R_e/pm	T_e/cm^{-1}	ν_s/cm^{-1}	E/cm^{-1}	R_e/pm	T_e/cm^{-1}	ν_s/cm^{-1}	E/cm^{-1}
		cis-$(H_2O)_3UO_2F_2$				*trans*-$(H_2O)_3UO_2F_2$				ref 25
$XA_1(0_g)$			178.16				177.74			
$aB_1(1_g)$	$^3\Delta_g$	21 903	184.96	20 769	714	22 708	184.57	21 542	720	18 797
$aA_2(1_g)$	$^3\Delta_g$	21 904	184.95	20 770	714	22 722	184.51	21 568	724	18 790
$aA_1(2_g)$	$^3\Delta_g$	23 874	185.13	22 667	719	23 393	184.79	22 143	724	19 541
$aB_2(2_g)$	$^3\Delta_g$	22 303	185.19	21 093	714	24 102	184.60	22 914	726	20 500
$bA_2(3_g)$	$^3\Delta_g$	24 591	185.37	23 299	720	24 934	185.07	23 583	724	21 523
$bB_1(3_g)$	$^3\Delta_g$	24 382	185.51	23 037	721	25 070	184.90	23 775	726	21 638
$bB_2(2_g)$	$^3\Phi_g$	26 080	186.27	24 363	737	26 927	186.43	24 990	731	24 243
$bA_1(2_g)$	$^3\Phi_g$	25 801	187.10	23 842	714	27 103	186.34	25 207	730	24 465
$cA_2(3_g)$	$^3\Phi_g$	28 868	186.34	27 134	735	29 079	185.76	27 383	742	26 291
$cB_1(3_g)$	$^3\Phi_g$	28 004	185.93	26 453	732	29 784	186.08	27 950	742	27 097
$cB_2(4_g)$	$^3\Phi_g$	31 186	186.80	29 325	719	32 068	186.72	30 046	722	29 497
$cA_1(4_g)$	$^3\Phi_g$	31 010	187.35	28 990	706	32 180	186.62	30 206	722	29 547

[a]See footnotes of Table 3.

dx.doi.org/10.1021/ic5006852 | Inorg. Chem. 2014, 53, 7340−7350

Table 12. Spectroscopic Data of the Luminescent States of $(H_2O)_nUO_2F_2$ (n = 0−3) from SO-Coupled CCSD(T) Calculations and Experimental Observations[a]

compds	state (Ω)	main	ΔR(U−O)/pm	E_{00}/cm^{-1}	$\nu_{s,e}$/cm^{-1}	$\nu_{s,g}$/cm^{-1}
UO_2F_2	1_g	$^3\Delta_g$	6.06	20 106	745	891
$(H_2O)_1UO_2F_2$	1_g	$^3\Delta_g$	6.20	20 773	744	868
cis-$(H_2O)_2UO_2F_2$	1_g	$^3\Delta_g$	6.74	20 433	720	854
cis-$(H_2O)_3UO_2F_2$	1_g	$^3\Delta_g$	6.80	20 704	714	845
trans-$(H_2O)_3UO_2F_2$	1_g	$^3\Delta_g$	6.81	21 476	720	852
theory	1_g	$^3\Delta_g$	6.80	21 000	720	850
exptl (at ∼6 K)[b]				20 074		849
exptl (RT)[c]				20 039	713	849

[a]See footnotes a and c of Table 6 and the Experimental Results section for experimental results. [b]At near liquid helium temperature. [c]At room temperature.

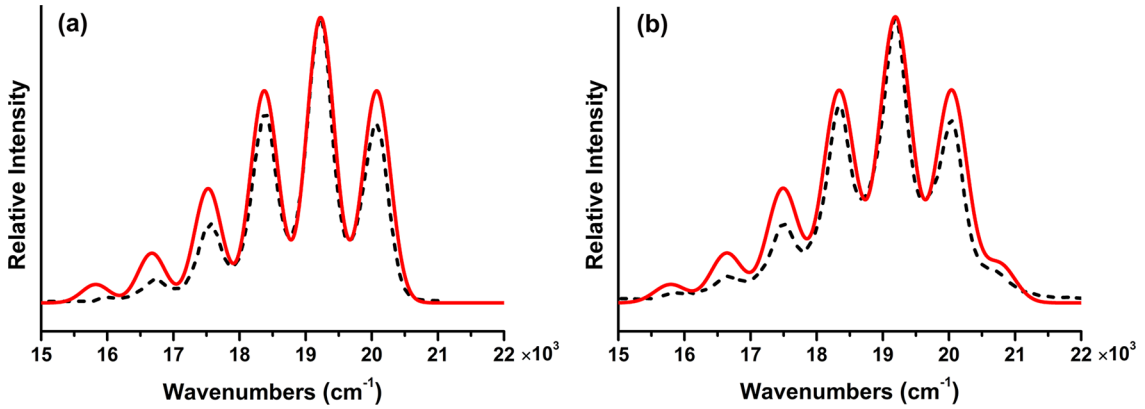

Figure 6. RASSCF/CCSD(T)/SO-simulated (red solid curve) and experimental (black dotted curve, see details in the Experimental Results section) luminescence spectra of UO_2F_2 in aqueous solution at pH = 3.0 with [U] = 3.6 × 10^{-5} M and [F$^-$] = 2.4 × 10^{-3} M under λ_{ex} = 415 nm: (a) simulation with bandwidth of 210 cm^{-1} and experiment at near liquid helium temperature 6 K and (b) simulation with bandwidth of 240 cm^{-1} and experiment at room temperature.

of electronic transitions. Our calculation results have shown that the oscillator strength for the second group of electronically excited states is higher than the first group ones, which is also found in the uranyl−glycine−water system.[12] The constraint C_{2v} symmetry used in aquo−UO_2F_2 system is expected to influence the accurate analysis on the oscillator strength. Therefore, we used the theoretically estimated thermal population of 9%, which includes the contribution from both the vibrationally and electronically excited states, to simulate the hot band in the room-temperature emission spectrum (see Figure 6b). Overall, our simulation results show good agreement with the experimental spectra, although the relative intensities of the other peaks except the most intense one are slightly higher than experimental ones. The small discrepancy in intensity distribution is probably due to the neglect of the contributions of UO_2F^+ and $UO_2F_3^-$ species, which account for ca. 20% of the total uranyl fluoride complexes and are also responsible for the band broadening.

In this work, we neglect the influence of the second solvation shell on the excited states and luminescence spectra, as it is not expected to significantly affect the above results, as analyzed below. According to our own experience and published literature on $UO_2(CO_3)_3^{5-}$, the water solvent effect on $UO_2(CO_3)_3^{5-}$ beyond the first coordination shell, when approximated by conductor-like polarizable model, presents the same electronic spectra pattern as that in the gas phase and slightly shifts transition energy within 1500 cm^{-1},[42] which is within the computational error bar of the method used in our work. Besides, according to the DFT-based Car−Parrinello molecular dynamics (CPMD) studies of aquo−uranyl−ligand complexes including nitrate, fluoride, and chloride by Bühl et al., the second solvation shell has insignificant effects on the geometrical structures of neutral uranyl complexes: the bond lengths R(U ← OH_2) and R(U ← ligand) change in opposite directions within 0.2 Å, whereas R(U−O_{ax}) changes little with the elongation less than 0.03 Å.[29,61] The almost negligible R(U−O_{ax}) difference indicates that the strength of the whole ligand field from the coordinated anionic ligands and water molecules changes little. Inasmuch as the excited state distributions and luminescent-state properties are solely determined by ligand field with the constant SO coupling effect in neutral aquo-UO_2F_2 complexes, the neglect of second solvation shell in this work will not considerably influence the excited state distributions and the simulated luminescence spectral shape. Despite the complexities of species distribution in solution, radiationless processes, and the approximations in computational simulation, our theoretically simulated luminescence spectrum reproduces experimental results reasonably well.

5. CONCLUSIONS

We have investigated the low-lying electronic spectra arising from $\sigma_u \rightarrow \delta_u,\phi_u$ transition and luminescence properties of UO_2F_2 in gas phase and its solvated complexes $(H_2O)_nUO_2F_2$ (n = 1−3) in aqueous solution. Excited-state calculation results of UO_2F_2 show that excitation energies and U−O bond length expansions from CASPT2-[g_1'] are lower than those from CCSD(T) by 1100 cm^{-1} and 0.6 pm, respectively. These differences are less obvious in the case of UO_2Cl_2,[13] probably due to the stronger coordination interaction of F$^-$ than Cl$^-$, thus requiring more accurate description of dynamic electron correlation in the $(H_2O)_nUO_2F_2$ species by using CCSD(T) method. The lowest excited states of UO_2F_2 are dominated by $^3\Delta_g$ type of configurations, in contrast to the leading $^3\Phi_g$ type in UO_2Cl_2,[13] showing the competition of SO coupling and ligand field effect in determining the energy level distribution.

dx.doi.org/10.1021/ic5006852 | Inorg. Chem. 2014, 53, 7340−7350

The luminescence spectrum of UO_2F_2 in gas phase is predicted on the basis of RASSCF/CASPT2-[g_1']/SO and RASSCF/CCSD(T)/SO results, respectively, by considering three symmetric vibration modes (i.e., O−U−O stretching, O−U−O bending, and F−U−F stretching). The simulated spectrum resembles that of UO_2Cl_2 as a result of the comparable U−O bond length change.

The influence of H_2O coordination on the electronic spectra and luminescent properties of UO_2F_2 has been investigated in details by comparisons among $(H_2O)_nUO_2F_2$ (n = 0−3) complexes using RASSCF/CCSD(T)/SO calculations. In contrast to the negligible Ar coordination influence on UO_2Cl_2, H_2O coordination changes the ordering of excited states of UO_2F_2 and weakens the U−O bond of the ground state and excited states, leading to an accompanying decrease of O−U−O symmetric stretching vibration frequency ν_s and expanding of the U−O bond length of excited states relative to that of the ground state. The changes above are due to the strong ligand field effect of H_2O, which destabilizes $^3\Phi_g$ far more than $^3\Delta_g$ state due to direct metal−ligand orbital overlap. When the number of coordinated water gradually increases toward saturation, excited-state energy level distributions converge with all the low-lying excited states dominated by $^3\Delta_g$ type and all the high-lying ones by $^3\Phi_g$ type, and the luminescent properties also go steadily with respect to adiabatic excitation energy, U−O bond length expansion and ν_s value of the ground state and the luminescent state. The luminescence spectra of UO_2F_2 in aqueous solution at both near liquid helium temperature and room temperature are simulated using the spectroscopic data of the luminescent state. When only the U−O symmetric stretching mode is considered, the simulation results agree well with the experimental spectra.

It should be pointed out that for accurate modeling of the electronic spectra of uranyl compounds, the knowledge of precise speciation and coordination environment of uranyl in the aqueous is critical. However, such information is difficult to obtain both experimentally and computationally. The speciation of uranyl in aqueous solution is influenced by several factors, including concentration, ionic strength, pH, and temperature, among others. A few uranyl species with different coordination numbers of anionic ligand and/or solvent molecules can coexist in the same solution condition, in spite of accounting for differential ratios. The ab initio (or first-principles) molecular dynamics (AIMD)-based approach has been used to treat the solvation problems of actinides, and related applications have confirmed that this method can reasonably reproduce geometrical parameters and energetics.[29,61,62] The synergy of experimental and theoretical investigations can give insights into the speciation and spectroscopic properties of uranyl compounds in condensed phase. Our study has demonstrated that detailed understanding of the excited states and luminescence property of uranyl systems is feasible via integrated theory and experiment.

AUTHOR INFORMATION

Corresponding Authors

*E-mail: sujing@sinap.ac.cn.
*E-mail: zheming.wang@pnnl.gov.
*E-mail: junli@tsinghua.edu.cn.

Notes

The authors declare no competing financial interest.

ACKNOWLEDGMENTS

The theoretical work was supported by NSFC (91026003, 21201106), the "Strategic Priority Research Program" of the Chinese Academy of Sciences (grant no. XDA02040104), and the National Basic Research Program of China (grant no. 2010CB934504). The calculations were performed at the Supercomputer Center of the Computer Network Information Center, Chinese Academy of Sciences, Tsinghua National Laboratory for Information Science and Technology, and Shanghai Supercomputing Center. A portion of the research was performed using EMSL, a national scientific user facility sponsored by the US Department of Energy's Office of Biological and Environmental Research and located at the Pacific Northwest National Laboratory, USA.

REFERENCES

(1) Rabinowitch, E.; Belford, R. L. *Spectroscopy and Photoechemistry of Uranyl Compounds*; Oxford University Press: Oxford, U.K., 1964.
(2) Su, J.; Li, J. *Prog. Chem.* **2011**, *23*, 1329−1337.
(3) Moulin, C.; Decambox, P.; Mauchien, P. *J. Radioanal. Nucl. Chem.* **1997**, *226*, 135−138.
(4) May, C. C.; Worsfold, P. J.; Keith-Roach, M. J. *Trends Anal. Chem.* **2008**, *7*, 160−168.
(5) Kirishima, A.; Kimura, T.; Tochiyama, O.; Yoshida, Z. *Radiochim. Acta* **2004**, *92*, 889−896.
(6) Wang, Z.; Zachara, J. M.; Yantasee, W.; Gassman, P. L.; Liu, C.; Joly, A. G. *Environ. Sci. Technol.* **2004**, *38*, 5591−5597.
(7) (a) Rutsch, M.; Geipel, G.; Brendler, V.; Bernhard, G.; Nitsche, H. *Radiochim. Acta* **1999**, *86*, 135−141. (b) Brachmann, A.; Geipel, G.; Bernhard, G.; Nitsche, H. *Radiochim. Acta* **2002**, *90*, 147−149. (c) Günther, A.; Geipel, G.; Bernhard, G. *Radiochim. Acta* **2006**, *94*, 845−851. (d) Günther, A.; Geipel, G.; Bernhard, G. *Polyhedron* **2007**, *26*, 59−65.
(8) (a) Szabó, Z.; Toraishi, T.; Vallet, V.; Grenthe, I. *Coord. Chem. Rev.* **2006**, *250*, 784−815. (b) Geipel, G. *Coord. Chem. Rev.* **2006**, *250*, 844−854.
(9) (a) Wolf, S. F. Trace Analysis of Actinides in Geological, Environmental, and Biological Matrices. In *The Chemistry of the Actinide and Transactinide Elements*; Morss, L. R., Edelstein, N. M., Fuger, J., Katz, J. J., Eds.; Springer: Dordrecht, 2006; Vol. *5*, pp 3273−3338. (b) Durbin, P. W. Actinides in Animals and Man. In *The Chemistry of the Actinide and Transactinide Elements*; Morss, L. R., Edelstein, N. M., Fuger, J., Katz, J. J., Eds.; Springer: Dordrecht, 2006; Vol. *5*, pp 3339−3440.
(10) Gorden, A. E. V.; Xu, J.; Raymond, K. N.; Durbin, P. W. *Chem. Rev.* **2003**, *103*, 4207−4282.
(11) Billard, I.; Geipel, G. *Springer Ser. Fluoresc.* **2008**, *5*, 465−492.
(12) Su, J.; Zhang, K.; Schwarz, W. H. E.; Li, J. *Inorg. Chem.* **2011**, *50*, 2082−2093.
(13) Su, J.; Wang, Y. L.; Wei, F.; Schwarz, W. H. E.; Li, J. *J. Chem. Theory Comput.* **2011**, *7*, 3293−3303.
(14) Su, J.; Dau, P. D.; Qiu, Y. H.; Liu, H. T.; Xu, C. F.; Huang, D. L.; Wang, L. S.; Li, J. *Inorg. Chem.* **2013**, *52*, 6617−6626.
(15) Su, J.; Schwarz, W. H. E.; Li, J. *Inorg. Chem.* **2012**, *51*, 3231−3238.
(16) Denning, R. G. *J. Phys. Chem. A* **2007**, *111*, 4125−4143.
(17) Pepper, M.; Bursten, B. E. *Chem. Rev.* **1991**, *91*, 719−741.
(18) Li, Y.; Su, J.; Mitchell, E.; Zhang, G. Q.; Li, J. *Sci. China: Chem.* **2013**, *56*, 1671−1681.
(19) Elam, K. R. Criticality Safety Study of UF_6 and UO_2F_2 in 8-in.-Diameter Piping, ORNL/TM-2003/239, UT-Battelle, LLC, Oak Ridge National Laboratory, Oak Ridge, TN, October 2003.
(20) Grigor'ev, G. Y.; Nabiev, S. S.; Malyugin, S. L.; Sukhanova, M. A.; Nadezhdinskii, A. I.; Ponurovskii, Y. Y. *At. Energy* **2008**, *105*, 280−289.
(21) (a) Kaminski, R.; Purcell, F. J.; Russavage, E. *Anal. Chem.* **1981**, *53*, 1093−1096. (b) Moriyasu, M.; Yokoyama, Y.; Ikeda, S. *J. Inorg.*

Nucl. Chem. **1977**, *39*, 2199−2203. (c) Billing, R.; Zakharova, G. V.; Atabekyan, L. S.; Henning, H. *J. Photochem. Photobiol., A* **1991**, *59*, 163−174. (d) Moulin, C.; Decambox, P.; Trecani, L. *Anal. Chim. Acta* **1996**, *321*, 121−126. (e) Azenha, M. E. D. G.; Burrows, H. D.; Formosinho, S. J.; Miguel, M. G. M.; Daramanyan, A. P.; Khudyakov, I. V. *J. Lumin.* **1991**, *48*−*49*, 522−526. (f) Beitz, J. V.; Williams, C. W. *J. Alloys Compd.* **1997**, *250*, 375−379.

(22) Vallet, V.; Wahlgren, U.; Schimmelpfennig, B.; Moll, H.; Szabó, Z.; Grenthe, I. *Inorg. Chem.* **2001**, *40*, 3516−3525.

(23) Gaillard, C.; El Azzi, A.; Billard, I.; Bolvin, H.; Hennig, C. *Inorg. Chem.* **2005**, *44*, 852−861.

(24) Tian, G.; Rao, L. *Inorg. Chem.* **2009**, *48*, 6748−6754.

(25) Wang, Q.; Pitzer, R. M. *J. Phys. Chem. A* **2001**, *105*, 8370−8375.

(26) Ruipérez, F.; Wahlgren, U. *J. Phys. Chem. A* **2010**, *114*, 3615−3621.

(27) Infante, I.; Visscher, L. *J. Comput. Chem.* **2004**, *25*, 386−392.

(28) Garcia-Hernandez, M.; Willnauer, C.; Krüger, S.; Moskaleva, L. V.; Rösch, N. *Inorg. Chem.* **2006**, *45*, 1356−1366.

(29) Bühl, M.; Sieffert, N.; Wipff, G. *Chem. Phys. Lett.* **2009**, *467*, 287−293.

(30) Odoh, S. O.; Walker, S. M.; Meier, M.; Stetefeld, J.; Schreckenbach, G. *Inorg. Chem.* **2011**, *50*, 3141−3152.

(31) AllisonJ. D.BrownD. S.Novo-GradacK. J. U.S. Environmental Protection Agency. MINTEQA2//PRODEFA2, A Geochemical Assessment Model for Environmental Systems (Version 4.0), Environmental Research Laboratory; HydroGeoLogic: Herndon, VA, 1998

(32) Guillaumount, R.; Fanghänel, T.; Neck, V.; Fuger, J.; Palmer, D. A.; Grenthe, I.; Rand, M. H. *Update on the Chemical Thermodynamics of Uranium, Neptunium, Plutonium, Americium and Technetium*; Elsevier: Amsterdam, 2003.

(33) Werner, H. J. MOLPRO, version 2008.1. Website: http://www.molpro.net.

(34) Bergner, A.; Dolg, M.; Kuechle, W.; Stoll, H.; Preuss, H. *Mol. Phys.* **1993**, *80*, 1431−1441.

(35) Energy-Consistent Pseudopotentials of the Stuttgart/Cologne Group. Website: http://www.theochem.uni-stuttgart.de/pseudopotential.

(36) Cao, X.; Dolg, M.; Stoll, H. *J. Chem. Phys.* **2003**, *118*, 487−496.

(37) Cao, X.; Dolg, M. *J. Mol. Struct.: THEOCHEM* **2004**, *673*, 203−209.

(38) Krishnan, R.; Binkley, J. S.; Seeger, R.; Pople, J. A. *J. Chem. Phys.* **1980**, *72*, 650−654.

(39) Francl, M. M.; Petro, W. J.; Hehre, W. J.; Binkley, J. S.; Gordon, M. S.; DeFrees, D. J.; Pople, J. A. *J. Chem. Phys.* **1982**, *77*, 3654−3665.

(40) Hariharan, P. C.; Pople, J. A. *Theor. Chim. Acta* **1973**, *28*, 213−222.

(41) Danilo, C.; Vallet, V.; Flament, J.-P.; Wahlgren, U. *Phys. Chem. Chem. Phys.* **2010**, *12*, 1116−1130.

(42) Ruipérez, F.; Danilo, C.; Réal, F.; Flament, J.-P.; Vallet, V.; Wahlgren, U. *J. Phys. Chem. A* **2009**, *113*, 1420−1428.

(43) Pierloot, K.; van Besien, E. *J. Chem. Phys.* **2005**, *123*, 204309.

(44) Roos, B. O.; Andersson, K. *Chem. Phys. Lett.* **1995**, *245*, 215−223.

(45) Roos, B. O.; Andersson, K.; Fülscher, M. P.; Serrano-Andrés, L.; Pierloot, K.; Merchán, M.; Molina, V. *J. Mol. Struct.: THEOCHEM* **1996**, *388*, 257−276.

(46) Malmqvist, P. Å.; Roos, B. O.; Schimmelpfennig, B. *Chem. Phys. Lett.* **2002**, *357*, 230−240.

(47) Roos, B. O.; Malmqvist, P. Å. *Phys. Chem. Chem. Phys.* **2004**, *6*, 2919−2927.

(48) (a) Wang, X. B.; Wang, Y. L.; Yang, J.; Xing, X. P.; Li, J.; Wang, L. S. *J. Am. Chem. Soc.* **2009**, *131*, 16368−16370. (b) Wang, Y. L.; Zhai, H. J.; Xu, L.; Li, J.; Wang, L. S. *J. Phys. Chem. A* **2010**, *114*, 1247−1254. (c) Wang, Y. L.; Wang, X. B.; Xing, X. P.; Wei, F.; Li, J.; Wang, L. S. *J. Phys. Chem. A* **2010**, *114*, 11244−11251. (d) Liu, H. T.; Xiong, X. G.; Dau, P. D.; Wang, Y. L.; Li, J.; Wang, L. S. *Chem. Sci.* **2011**, *2*, 2101−2108.

(49) (a) Dau, P. D.; Su, J.; Liu, H. T.; Liu, J. B.; Huang, D. L.; Li, J.; Wang, L. S. *Chem. Sci.* **2012**, *3*, 1137−1146. (b) Dau, P. D.; Su, J.; Liu, H. T.; Huang, D. L.; Li, J.; Wang, L. S. *J. Chem. Phys.* **2012**, *137*, 064315.

(50) Fonger, W. H.; Struck, C. W. *J. Chem. Phys.* **1974**, *60*, 1994−2002.

(51) Frisch, M. J.; Trucks, G. W.; Schlegel, H. B.; Scuseria, G. E.; Robb, M. A.; Cheeseman, J. R.; Montgomery, J. A., Jr.; Vreven, T.; Kudin, K. N.; Burant, J. C.; Millam, J. M.; Iyengar, S. S.; Tomasi, J.; Barone, V.; Mennucci, B.; Cossi, M.; Scalmani, G.; Rega, N.; Petersson, G. A.; Nakatsuji, H.; Hada, M.; Ehara, M.; Toyota, K.; Fukuda, R.; Hasegawa, J.; Ishida, M.; Nakajima, T.; Honda, Y.; Kitao, O.; Nakai, H.; Klene, M.; Li, X.; Knox, J. E.; Hratchian, H. P.; Cross, J. B.; Bakken, V.; Adamo, C.; Jaramillo, J.; Gomperts, R.; Stratmann, R. E.; Yazyev, O.; Austin, A. J.; Cammi, R.; Pomelli, C.; Ochterski, J. W.; Ayala, P. Y.; Morokuma, K.; Voth, G. A.; Salvador, P.; Dannenberg, J. J.; Zakrzewski, V. G.; Dapprich, S.; Daniels, A. D.; Strain, M. C.; Farkas, O.; Malick, D. K.; Rabuck, A. D.; Raghavachari, K.; Foresman, J. B.; Ortiz, J. V.; Cui, Q.; Baboul, A. G.; Clifford, S.; Cioslowski, J.; Stefanov, B. B.; Liu, G.; Liashenko, A.; Piskorz, P.; Komaromi, I.; Martin, R. L.; Fox, D. J.; Keith, T.; Al-Laham, M. A.; Peng, C. Y.; Nanayakkara, A.; Challacombe, M.; Gill, P. M. W.; Johnson, B.; Chen, W.; Wong, M. W.; Gonzalez, C.; Pople, J. A. *Gaussian 03*, revision B.05; Gaussian, Inc.: Wallingford, CT, 2003.

(52) Wilson, E. B.; Decius, J. C.; Cross, P. C. *Molecular Vibrations: The Theory of Infrared and Raman Vibrational Spectra*; McGraw-Hill: New York, 1955.

(53) (a) McIntosh, D. F.; Peterson, M. R. General Vibrational Analysis Programs for Personal Computers; 4 FORTRAN Computer Programs: UMAT, BMAT, ATOM2, FFIT. Q.C.P.E. Bulletin. Quantum Chemistry Program Exchange. Department of Chemistry, Indiana University: Bloomington, IN, 1989; Vol. 9, No 3, pp 47102−47405. Website: http://qcpe@indiana.edu. (b) McIntosh, D. F. *Theor. Chem. Acc.* **2010**, *125*, 177−184.

(54) Huang, K.; Rhys, A. *Proc. R. Soc. London* **1950**, *204A*, 406−423.

(55) Chang, H.-S.; Korshin, G. V.; Wang, Z.; Zachara, J. M. *Environ. Sci. Technol.* **2006**, *40*, 1244−1249.

(56) van Besien, E.; Pierloot, K.; Görller-Walrand, C. *Phys. Chem. Chem. Phys.* **2006**, *8*, 4311−4319.

(57) Matsika, S.; Pitzer, R. M. *J. Phys. Chem. A* **2001**, *105*, 637−645.

(58) Tecmer, P.; Bast, R.; Ruud, K.; Visscher, L. *J. Phys. Chem. A* **2012**, *116*, 7397−7404.

(59) Su, J.; Wei, F.; Schwarz, W. H. E.; Li, J. *J. Phys. Chem. A* **2012**, *116*, 12299−12304.

(60) First, the peak intensities of the experimental spectrum were normalized relative to the most intense band, and the intensity of the most intense band was set to 1. Then, the same treatment was applied to the theoretical spectrum. The bandwidth in the simulation was obtained by fitting that of the most intense band to be consistent with the experimental result.

(61) (a) Bühl, M.; Kabrede, H.; Diss, R.; Wipff, G. *J. Am. Chem. Soc.* **2006**, *128*, 6357−6368. (b) Bühl, M.; Sieffert, N.; Golubnychiy, V.; Wipff, G. *J. Phys. Chem. A* **2008**, *112*, 2428−2436.

(62) (a) Atta-Fynn, R.; Bylaska, E. J.; Schenter, G. K.; de Jong, W. A. *J. Phys. Chem. A* **2011**, *115*, 4665−4677. (b) Spezia, R.; Beuchat, C.; Vuilleumier, R.; D'Angelo, P.; Gagliardi, L. *J. Phys. Chem. B* **2012**, *116*, 6465−6475. (c) Atta-Fynn, R.; Bylaska, E. J.; de Jong, W. A. *J. Phys. Chem. Lett.* **2013**, *4*, 2166−2170.